Removal of tetracycline from aqueous solution by *azolla*, fig leaves, eggshell and egg membrane modified with magnetite nanoparticles

Naereh Besharati[a,b,*], Nina Alizadeh[a], Shahab Shariati[c]

[a]*Department of Chemistry, Guilan University, Rasht*

[b]*Guilan Agricultural and Natural Resources Research and Education Center, Agricultural Research, Education and Extension Organization (AREEO), Rasht, Iran, Tel. +989111321359; emails: Naerehb@yahoo.com (N. Besharati), n-alizadeh@guilan.ac.ir (N. Alizadeh)*

[c]*Department of Chemistry, Rasht Branch, Islamic Azad University, Rasht, Iran, email: shariaty@iaurasht.ac.ir*

ABSTRACT

Nowadays, antibiotics are used in large amount to care animals and humans. Tetracycline (TC) is widely used as an antibiotic and most of it is discharged into the water environment. In this study, the adsorption of TC by magnetite nanoparticles loaded eggshell (MNLES), egg membrane (MNLEM), azolla (MNLA) and fig leaves (MNLFL) as facile, economic and cheap adsorbents were studied. MNLES, MNLEM, MNLA and MNLFL were prepared with chemical co-precipitation method and were characterized with Fourier-transform infrared spectroscopy, X-ray diffraction, scanning electron microscopy and energy-dispersive X-ray instruments. The dose of adsorbents, pH of solution, ionic strength and contact time were examined and optimized as experimental variables affecting TC removal. Kinetic and equilibrium data for TC adsorption on each of the studied adsorbents were obtained. Pseudo-first-order, pseudo-second-order, intraparticle diffusion and Elovich kinetic models were studied for investigating the kinetic of adsorption. At the optimum conditions, the sorption of the TC on the MNLES, MNLEM, MNLA and MNLFL adsorbents were best described by pseudo-second-order kinetic model. The equilibrium data of MNLES for TC adsorption were fitted well to Freundlich isotherm whereas the data of MNLEM, MNLA and MNLFL for TC adsorption were fitted the Langmuir isotherm. The results showed that MNLEM can be used as efficient adsorbent for removal of TC from aqueous solutions. It was found that MNLES and MNLFL have TC adsorption less than MNLEM and also MNLA did not considered as a good adsorbent for TC removal.

Keywords: Tetracycline; Eggshell; Egg membrane; Azolla; Fig leaves, Magnetite nanoparticles

1. Introduction

Antibiotics especially tetracyclines are the most important pharmaceutical pollutants that enter in water environment. Industries that manufacture these drugs and also medicinal uses in humans and animals are sources of pollution [1,2]. Nowadays, different methods such as photolysis, ion-exchange, ozonation and adsorption are used for TCs degradation or removal in water and wastewater treatment [3]. Between them, adsorption is a useful method because of its efficiency and affordable benefits [4–6]. Up to now, different adsorbents were used for TC removal including activated carbon [7], graphene oxide [8], resins [9], magnetite [4–6], chitosan [10] and clays [11]. The use of magnetic sorbents to remove contaminants has particular importance due to the ease of attraction in the magnetic field, speed and economics [2–12].

Today, we see an increase in azolla in ponds, farms and in the aquatic environment as a source of pollution. On the other hand, fig tree is abundant in the northern regions of

* Corresponding author.

Iran, so, large quantities of fig leaves are available. Also, large amount of eggs are consumed daily in the world. The eggshell is thrown away that can be used without any cost, as well as egg membrane. Therefore, all selected natural adsorbents have no cost. Natural matters modified with magnetite nanoparticles are used as new adsorbents for adsorption of environment pollutants because of their large surface area, cheapness, sufficient stability, easy to preparation, non-toxicity and high adsorption efficiency [4–6,13–16]. Between different methods for preparation of magnetite (Fe_3O_4) nanoparticles (MNPs), co-precipitation was selected because of its facility to produce iron oxide from iron ion solution [17–19]. So, this study focused on eggshell, egg membrane, azolla and fig leaves modified with magnetite nanoparticles as adsorbents for TC removal. The amounts of adsorbents, pH of solution, ionic strength and contact time were examined to determine optimum conditions to obtain highest TC removal efficiency. Pseudo-first-order, pseudo-second-order, Elovich and intraparticle diffusion models were examined for kinetic adsorption and equilibrium data were evaluated based on Langmuir, Freundlich and Temkin isotherm models.

2. Experimental

2.1. Reagents and materials

TC (Fig. 1) was obtained from Merck (Darmstadt, Germany). Analytical reagent grade was selected for all materials and reagents. Double distilled water (DW) was used for dilution of solutions and also calibration curve was plotted using proper concentrations of TC in DW. Ferric chloride hexahydrate ($FeCl_3 \cdot 6H_2O$), ferrous chloride heptahydrate ($FeCl_2 \cdot 7H_2O$), ammonia (NH_3, 28 wt.%), hydrochloric acid (37 wt.%) and sodium hydroxide were prepared from Merck. Stock solutions of TC (C_{TC} = 44 mg L^{-1}) were prepared in DW for optimization studies.

2.2. Instrumentation

A Jenway pH meter (model 370, England) for adjustment the pH of solutions, single beam spectrophotometer (Jenway, model 6105, England) for measuring the absorbance of TC solution, scanning electron microscopy (SEM, model EM3200, USA) for study the surface morphology and particle size, X-ray diffraction (XRD, Philips, model X'PERT MPD, Netherlands) using CuKα radiation source with 2θ range of 0.5°–70° and Fourier-transform infrared

spectroscopy (FT-IR, Bruker, model Alfa, Germany) for study the structure of MNPs were used. Also, coffee grinder (model MCG 1575, China) and magnetic stirrer (Heidolph MR3001, USA) were utilized and for magnetic separation a strong super magnet (1 cm × 3 cm × 5 cm) with 1.4 T magnetic field was applied.

2.3. Preparation of the adsorbents

Azolla *filiculoides* were obtained from fish ponds in Keshelvarzal, Rasht, Iran. The egg was prepared from store and fig leaves were collected from trees in Rasht, Iran. Eggshell and egg membrane were collected, washed with DW and dried in the oven at 105°C. Then, they were sieved to 150–200 μm particle size and were dried at 105°C for 24 h to remove moisture and stored in a closed bottle for later use in adsorption studies [20].

The azolla was washed with DW and dried in sun. They were then powdered and sieved for using as a biosorbent and dried in oven at 100°C and milled in a coffee mill. The particles smaller than 0.5 mm were stored in order to modify their surface [21].

For fig leaves, 10 g of fig leaves were stirred in 2 L DW strongly (at a speed of 40 rpm) at 25°C ± 1°C during 4 h, then filtered, washed with DW to remove the surface sticky particles and water soluble materials, and dried in oven at 80°C for 24 h after filtration. These materials were crushed and sieved (>0.125 mm), for further batch sorption experiments [22].

2.4. Preparation of magnetite nanoparticle loaded natural adsorbents

Magnetite nanoparticles loaded eggshell (MNLES), egg membrane (MNLEM), magnetite nanoparticle loaded azolla (MNLA) and magnetite nanoparticle loaded fig leaves (MNLFL) were synthesized using co-precipitation method. $FeCl_3 \cdot 6H_2O$ (6.1 g) and $FeCl_2 \cdot 4H_2O$ (4.2 g) were dissolved in 100 mL DW and heated to 90°C. 10 mL ammonia solution (28 wt.%) and 1 g of natural adsorbents powders (separately for preparation of MNLES, MNLEM, MNLA and MNLFL) were rapidly added to 200 mL of DW. The pH of the reaction medium was adjusted to 10. The mixture was stirred at 80°C for 30 min and then cooled to room temperature. The black precipitates of natural adsorbents modified with magnetite nanoparticles were collected, washed with DW, dried at 50°C (24 h) and finally stored for further use [22]. It is clearly observed that all the MNLES, MNLEM, MNLA and MNLFL were attracted by the magnet due to the good magnetic behaviour of the synthesized nanoparticles.

2.5. TC adsorption optimization

In primary experiments, the UV-Vis absorption of TC at various pHs were studied with measuring absorbance of TC solution (44 mg L^{-1}) at 358 nm to study the effect of solution pH on the absorption behaviour of TC. Various experimental parameters affecting the TC removal efficiency were studied and optimized to achieve maximum adsorption efficiency. For optimization studies, 0.03 g of
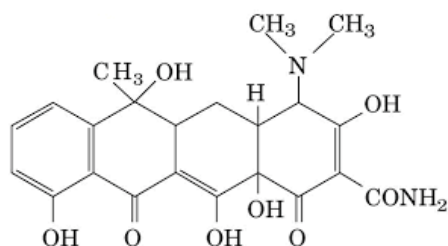
Fig. 1. Chemical structure of Tetracycline

each adsorbent was separately added to 20 mL solution containing TC in a 50 mL beaker. The pH of each solution was adjusted to the desired value using 0.1 mol L^{-1} HCl or NaOH solutions and the mixture was stirred rapidly for 30 min. After TC adsorption, adsorbent was quickly separated from the sample solutions by using the super magnet (1.4 T). The TC residual concentrations in the supernatant clear solution were determined with spectrophotometer using the proper calibration curve. The following equation was applied to calculate the TC removal efficiency in the experiments:

$$\%R = \frac{C_0 - C_t}{C_0} \times 100 \tag{1}$$

where C_0 and C_t are the initial and residual concentrations of TC after removal by synthesized adsorbents.

3. Result and discussion

3.1. Characterization of the synthesized MNPs

Characterization of the synthesized MNLES, MNLEM, MNLA and MNLFL were studied using XRD and SEM instruments. Fig. 2 shows the SEM images of the pre-treated eggshell, egg membrane, azolla, fig leaves and synthesized magnetic adsorbents (MNLES, MNLEM, MNLA and MNLFL). Images indicated that surface of natural adsorbents were modified with magnetite nanoparticles to create magnetic properties.
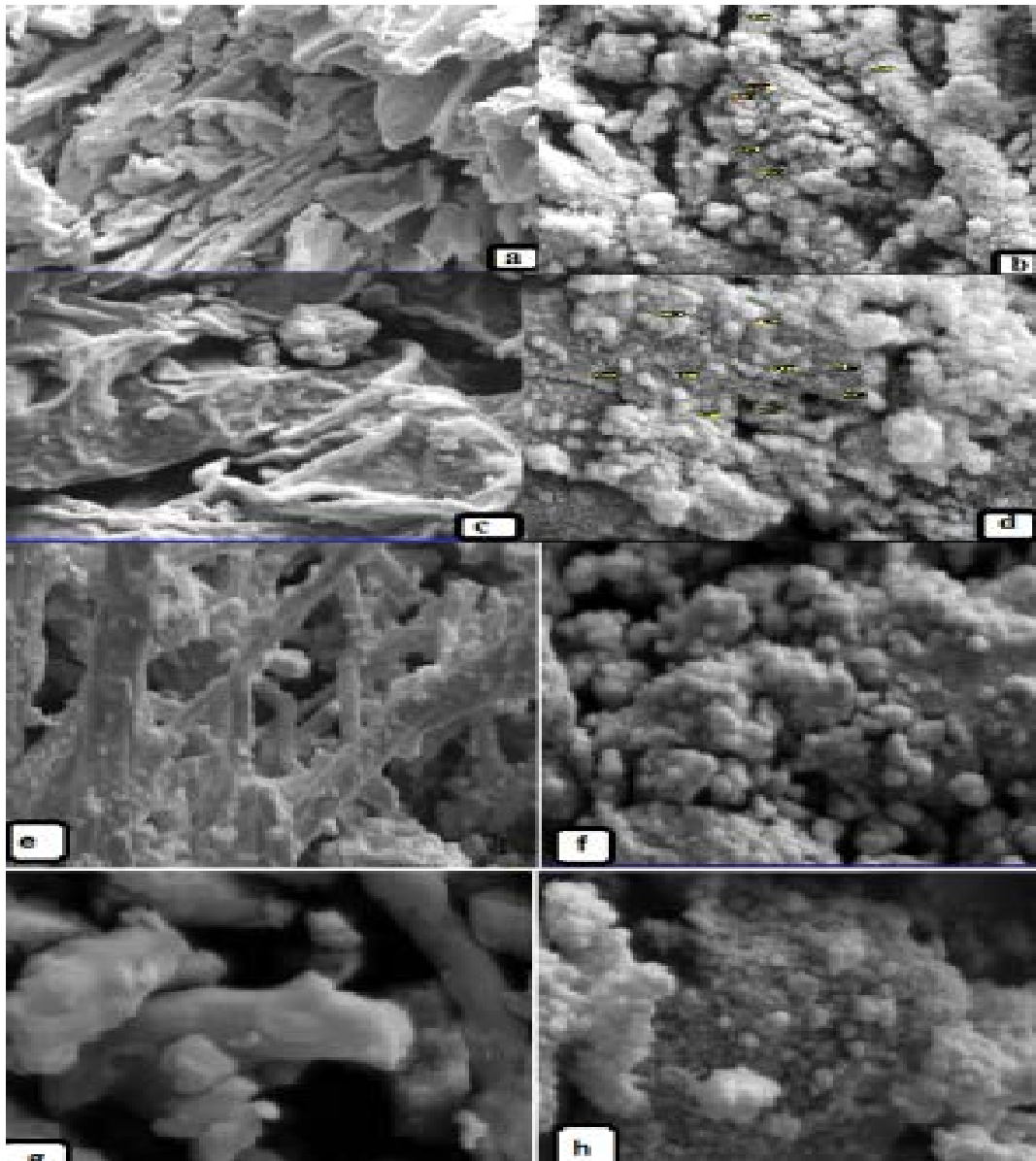
Fig. 2. The SEM image of (a) pretreated fig leaf, (b) MNLFL, (c) pretreated azolla, (d) MNLA, (e) pretreated egg shell, (f) MNLES, (g) pretreated egg membrane, and (h) MNLEM.

The XRD pattern of pre-treated natural adsorbents, MNLES, MNLEM, MNLA and MNLFL are shown in Fig. 3.

As the XRD patterns of MNLES and MNLEM show, the typical peaks of Fe_3O_4 can be observed. According to this figure, the diffraction peaks at $2\theta = 34.32°, 42.14°, 46.11°,$ 50.76° and 55.88° for MNLES, $2\theta = 35.36°, 41.65°, 50.70°,$ 67.72° and 74.72° for MNLEM and $2\theta = 35.2°, 41.5°, 50.6°$ and 63.2°, 67.7°, 74.7° for MNLFL and MNLA are matched well with the XRD pattern of pure magnetite. The results confirm that Fe_3O_4 nanoparticles are successfully impregnated onto the surfaces of natural adsorbents.

The FT-IR spectra of both modified and unmodified eggshell, egg membrane, azolla and fig leaves are shown in Fig. 4.

The spectra display absorption bands, indicating the complex nature of natural adsorbents as well as the bands related to the magnetite nanoparticles. FT-IR spectroscopic analysis of pre-treated eggshell and egg membrane indicated broad bands at 3,420 cm⁻¹, representing surface bonded –OH groups. The band observed at about 2,850–2,920 cm⁻¹ could be assigned to the aliphatic C–H groups. The strong band at 1,638–1,648 cm⁻¹ represents the C=C stretching vibrations, absorption band around 1,380–1,415 cm⁻¹ represents S=O stretching of sulphate. The band observed at about 870 and 710 cm⁻¹ could be assigned to the alkene C=C bond. The FT-IR of azolla and fig leaves indicated broad band at 3,420 cm⁻¹, representing bonded –OH groups and aliphatic C–H group at 2,850–2,920 cm⁻¹. At wave numbers around 1,720 cm⁻¹ a shoulder is observed which may be related to the stretching vibrations of carbonyl in carboxyl group. The bands at 1,620–1,630 cm⁻¹ represent the C–O stretching vibration conjugated with the NH_2 (amide 1 band). Absorption bands around 1,380 cm⁻¹ represent alkyl group. The band observed at about 1,000–1,100 cm⁻¹ could be assigned to the aliphatic C–N band. The spectra in Fig. 4 shows that there were almost the same functional
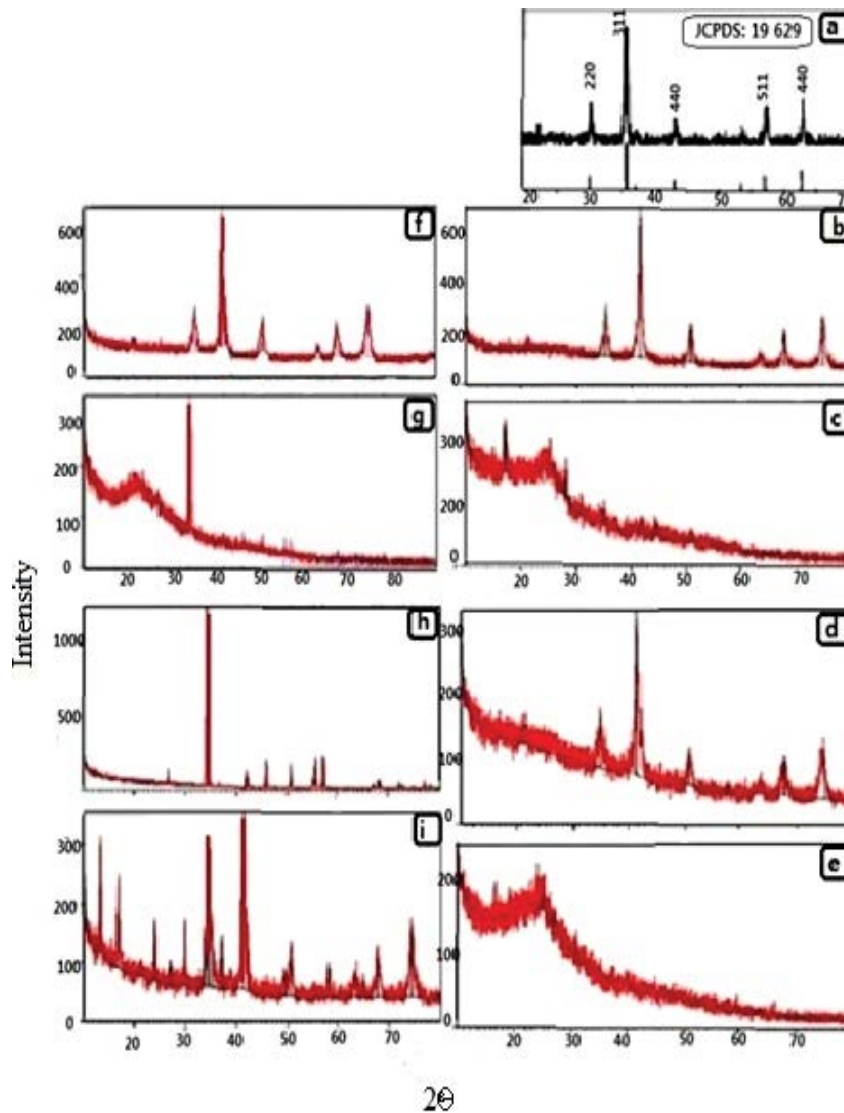
Fig. 3. XRD pattern of (a) Fe_3O_4, (b) pretreated fig leaf, (c) MNLFL, (d) pretreated azolla, (e) MNLA, (f) pretreated egg membrane, (g) MNLEM, (h) pretreated egg shell, and (i) MNLES.
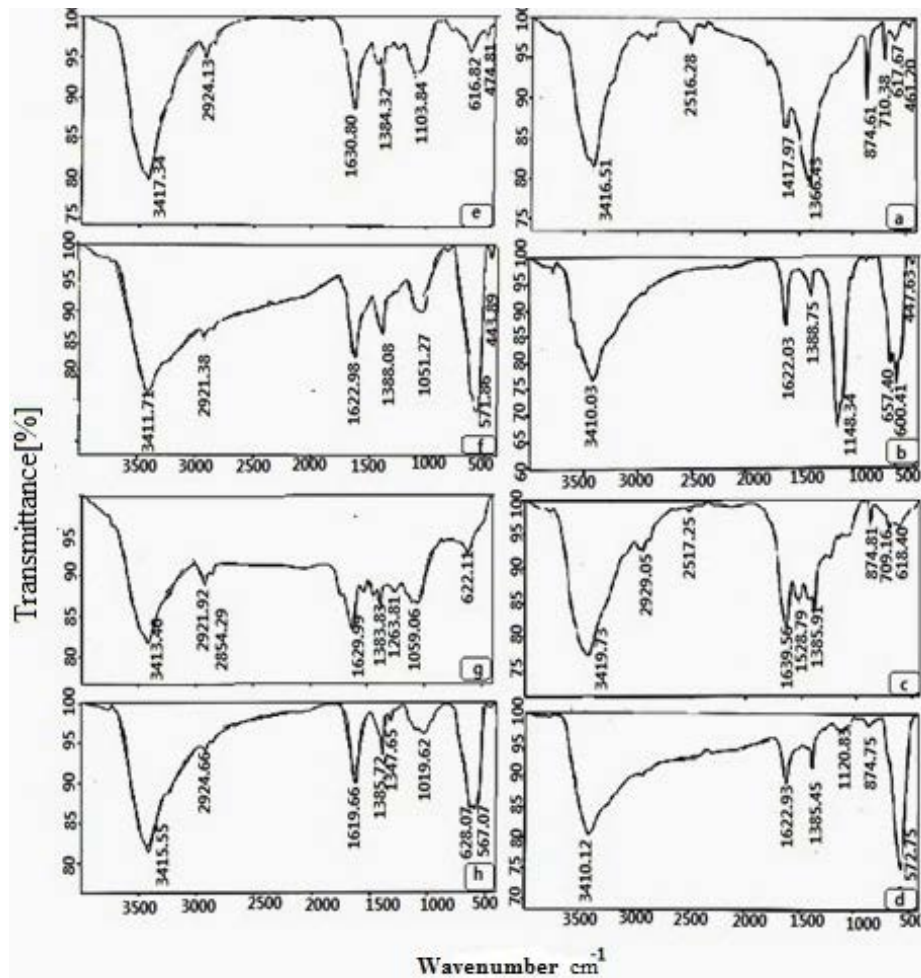
Fig. 4. FT-IR spectra of (a) pretreated egg shell, (b) MNLES, (c) pretreated egg membrane, (d) MNLEM, (e) pretreated fig leaf, (f) MNLFL, (g) pretreated azolla, and (h) MNLA.

groups on the surface of MNLA, MNLFL, MNLES and MNLEM. Stretching of Fe–O at 1,019–1,150 cm^{-1}, O–H at 1,330–1,420 cm^{-1}, stretching and bending vibrations of O–H at 1,632 and 3,446 cm^{-1}, stretching vibrations of Fe–O at 500–1,000 cm^{-1} are in agreement with the magnetite spectrum. Thus, all the above results indicate that the magnetic nanoparticles were loaded on the natural adsorbents.

As shown in Fig. 5, energy-dispersive X-ray spectroscopy (EDX) analysis revealed that MNLES and MNLEM have 34.57% and 20.75% Fe that means 1 g MNLES and MNLEM have 0.47 and 0.28 g Fe$_3$O$_4$, respectively. Also, EDX analysis revealed that MNLFL and MNLA have 33.48% and 26.36% Fe which means the presence of 0.46 and 0.36 g of Fe$_3$O$_4$ in 1 g of MNLFL and MNLA, respectively. These analyses confirm the presence of iron oxide in the synthesized natural adsorbents.

3.2. Optimization the experimental parameters

3.2.1. Effect of adsorbent amount on the TC removal efficiency

The adsorption process is significantly affected by the adsorbent amount because it is related to the adsorption capacity. The dependence of the TC adsorption on the amount of adsorbents was studied at room temperature by varying the adsorbent amount from 0.01– 0.06 g (0.5–3 g L^{-1}) in contact with 20 mL solution (C_{TC} = 44 mg L^{-1}, pH = 7). According to the Fig. 6, 0.02 g (1 g L^{-1}) of MNLES and MNLEM and 0.01 g (0.5 g L^{-1}) of MNLA and MNLFL showed the maximum TC removal efficiencies. TC removal efficiency was increased by increasing the contact surface of the adsorbents with TC and the greater availability of the adsorbents. As the amount of adsorbent increases, the number of sites available for adsorption increases. On the other hand, at high adsorbent amounts, the adsorption sites remain unsaturated during the adsorption process, reducing the amount of TC adsorbed per unit mass of adsorbent.

3.2.2. Effect of contact time on the TC removal efficiency

Effect of contact time on the TC adsorption was studied to determine necessary time by adsorbents to remove TC (44 mg L^{-1}) from solution. Absorbance of the residual solution at λ_{max} = 358 nm was measured at different times. It was observed that 59% and 44.4% of TC were adsorbed by MNLEM and MNLFL after 45 min, respectively. TC removal
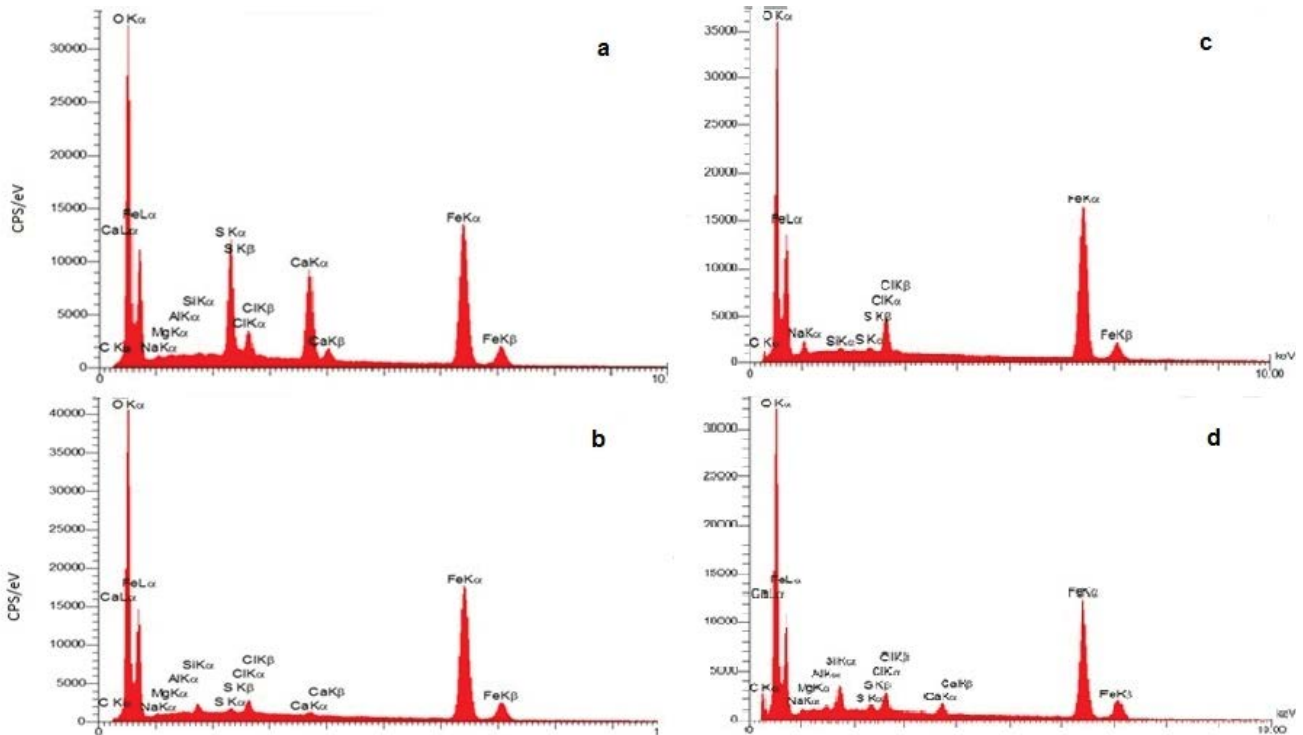
Fig. 5. EDX of (a) MNLEM, (b) MNLES, (c) MNLFL, and (d) MNLA
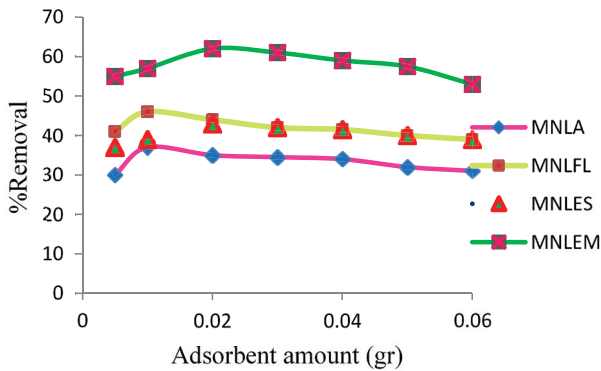
Fig. 6. Effect of amount of adsorbents on the removal efficiency of TC (C_{TC} = 44 mg L^{-1}; V = 20 mL).

efficiency was changed from 40% to 41.5% by MNLES with changing contact time from 45 to 55 min. Also, MNLA showed low removal efficiency as 33.7% at 55 min and had not good removal for TC (Fig. 7). So, agitation time of 45 min was selected as optimum time.

3.2.3. Effect of pH on the TC removal efficiency

Changes in the solution pH affect surface adsorption because of its effect on the dissociation of groups at the active surface of the adsorbents and functional groups of TC. The effect of pH on TC adsorption was done in the pH range of 3 to 12 depending on the surface charge of magnetic nanoparticles and pK_a values of TC and because of

three acid dissociation constants of TC that start at pH = 3.30. For this purpose, 0.01 g of adsorbents was added to 20 mL of 44 mg L^{-1} TC solution at different pHs in the range of 3 to 12.

TC is an amphoteric molecule. So, it has three acid dissociation constants (3.30, 7.68 and 9.68) that are related to the tricarbonyl, dimethyl amine and β-diketone groups, respectively [23]. In pH less than 3.30, H$_4$TC$^+$ ions are the main form in the solution due to the protonation of dimethyl amine group. As the pH increases, they become uncharged as zwitter ionic form (TC) and then changed to anionic forms. In the pH range of 3.30–7.68, dimethyl amine group and a negatively charged hydroxyl group are the forms of TC and H$_3$TC as the main form and tetracycline presents as a zwitter ion, due to the loss of a proton. When the pH rises to 7.68–9.69, H$_2$TC$^-$ ions are the dominant form of TC. In the pH value upper than 9.69, TC is mainly in the form of HTC^{2-} due to the loss of protons from the tri-carbonyl system and phenolic diketone moiety [24,25].

As pH increases from 5.0 to 8.5, the dominant species of TC changed from being neutral or zwitterion to negatively charged (Fig. 8). Electrostatic repulsion between similar charges of TC and MNPs was greater at either lower pHs (positive-positive repulsion) or higher pHs (negative-negative repulsion), thus creating a maximum electrostatic attraction at the intermediate pHs range [26].

Results show that in the pH range of 3 to 9, adsorption of TC on natural adsorbents decreases slowly but in greater pHs, more decrease in removal is occurred that is related to the repulsion of negative form of TC with negative surface of the adsorbents. Therefore, pH = 7.0 was chosen as optimum pH for further experiments.
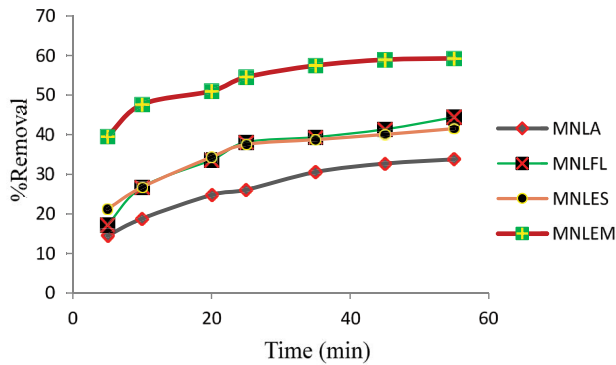
Fig. 7. Effect of contact time on the removal efficiency of TC (C_{TC} = 44 mg L^{-1}; V = 20 mL).
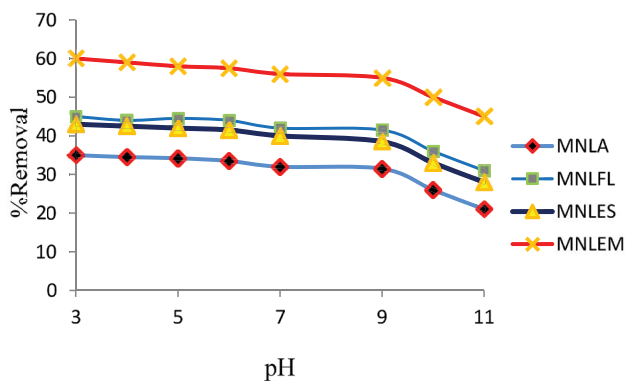
Fig. 8. Effect of pH of solution on the TC removal (C_{TC} =44 mg L^{-1}; V = 20 mL).

3.2.4. Effect of NaCl concentration on the TC removal efficiency

Effect of ionic strength on TC removal was studied with different concentrations of NaCl (0–0.1 M). Fig. 9 shows that increasing the NaCl concentration has not any significant effect on TC removal efficiency. Also, it indicated that adsorption of TC on the magnetite modified natural adsorbents is independent of ionic strength of solution [4,27].

3.3. Study of kinetic and adsorption isotherms

The kinetic parameters, which are helpful for the prediction of the adsorption rate, give important information for designing and modelling of the adsorption processes and we can select optimum operating conditions for removal processes. In order to predict controlling mechanism for adsorption onto adsorbents, pseudo-first-order, pseudo-second-order, Elovich and intraparticle diffusion models were studied. Correlation coefficients (R^2 values close to 1) were used for expression correlation between experimental data and the kinetic models. In the present study, kinetic studies were performed in the time intervals ranged from 0 to 55 min. After contact between the adsorbents (separately) and TC during the time intervals, the residual TC concentration was measured with
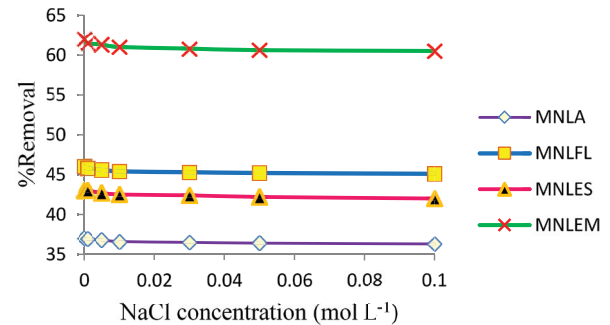
Fig. 9. Effect of NaCl concentration on removal of TC (C_{TC} = 44 mg L^{-1}; V = 20 mL).

spectrophotometer at 395 nm. Fig. 10 shows the equilibrium concentrations of TC at the adsorption time interval of 5–45 min. The TC residual concentration in the solution was monitored and the adsorption capacity at time t (q_t, mg g^{-1}) was calculated by the following equation:

$$q_t = \frac{(C_0 - C_t) \times V}{W} \tag{2}$$

where C_0 and C_t are the initial and equilibrium concentrations (mg L^{-1}) of TC at a given time t, respectively. Also, V is the solution volume (L) and W is the weight of the adsorbent (g). The removal rate was very fast during the initial stages of the adsorption process. The kinetic of adsorption was obtained as pseudo-second-order according to following equation. The pseudo-second-order reaction rate may be dependent on the amount of solute adsorbed on the surface of adsorbent and the amount adsorbed at equilibrium. The kinetic rate equations for pseudo-second-order reaction can be written as follows:

$$\frac{t}{q_t} = \frac{1}{K_2 q_e^2} + \left[\frac{1}{q_e}\right] t \tag{3}$$

where q_t and q_e are the values of adsorbed TC at each time and at equilibrium and K_2 (g mg^{-1} min^{-1}) is the pseudo-second-order rate constant. If the second-order kinetic equation is applicable, the plot of t/q_t against t (Eq. (3)) should give a linear relationship. The q_e and K_2 can be determined from the slope and intercept of the plot. Fitting of kinetic data to pseudo-second-order kinetic model, was shown in Fig. 10 and Table 1.

Pseudo-second-order kinetic model was confirmed with higher correlation coefficient values (R^2 > 0.9912) rather than pseudo-first-order kinetic model (R^2 < 0.6328). Hence, pseudo-second-order kinetic model was more valid to describe the adsorption behaviour of TC on MNLEM, MNLES, MNLA and MNLFL. It shows that the TC adsorption followed by chemisorption mechanism via electrostatic attraction.

Fig. 11 shows the intraparticle diffusion model.

If the intraparticle diffusion model is involved in the adsorption process, the graph will be linear. If the drawn

line passes through the origin, the intraparticle diffusion is the controller step, but if the line doesn't pass through the origin, it indicates that some degree of control is the boundary layer and the intraparticle penetration is not the only controller step and other processes may control the rate of adsorption. So, we conclude that this model isn't controller.

Equilibrium isotherm equations are used to describe the experimental sorption data. The parameters obtained from the different models provide important information on the sorption mechanisms and the surface properties and affinities of the sorbent. The equilibrium adsorption isotherm was determined using batch studies. 20 mL of the TC solution with various initial TC concentrations were poured into a beaker. The time required to reach equilibrium as determined in equilibrium studies was 55 min. The amount of TC uptake by the MNLA, MNLFL, MNLES and MNLEM, q_e (mg g^{-1}), was obtained by Eq. (2).

Adsorption data obtained in a concentration range of 10–50 mg L^{-1} were correlated with the following linear forms of Langmuir (Eq. (4)) [28], Freundlich (Eq. (5)) [29] and Temkin (Eq. (6)) [30].

Adsorption isotherm models:

Langmuir equation:

$$\frac{C_e}{q_e} + \frac{1}{K_l q_{max}} + \frac{1}{q_{max}} C_e \tag{4}$$

Freundlich equation:

$$\log q_e = \log K_f + \frac{1}{n} \log C_e \tag{5}$$

Temkin equation:

$$q_e = K_1 \cdot \ln(K_2) + K_1 \cdot \ln(C_e) \tag{6}$$

where q_e is the equilibrium TC concentration on the adsorbent (mg g^{-1}), C_e is the equilibrium TC concentration in the solution (mg L^{-1}), q_{max} is the monolayer capacity of the adsorbent (mg g^{-1}), K_L is the Langmuir constant (L mg^{-1}) and is related to the free energy of adsorption, K_F is the Freundlich constant (L g^{-1}) and n (dimensionless) is the heterogeneity factor.

In the Langmuir model, a plot of C_e/q_e vs. C_e should indicate a straight line with slope $1/q_{max}$ and an intercept of $1/(K_L q_{max})$. K_1 is related to the heat of adsorption (L g^{-1}) and K_2 is the dimensionless Temkin isotherm. The correlation coefficient for the study of TC adsorption isotherm on the MNLFL ($R^2_{Langmuir} = 0.9932$, $R^2_{Freundlich} = 0.777$), MNLA ($R^2_{Langmuir} = 0.9991$, $R^2_{Freundlich} = 0.6595$) and MNLEM ($R^2_{Langmuir} = 0.9956$, $R^2_{Freundlich} = 0.8905$) (Table 2) adsorbents showed strong positive evidence that TC adsorption follows the Langmuir isotherm (Fig. 12). This indicates that
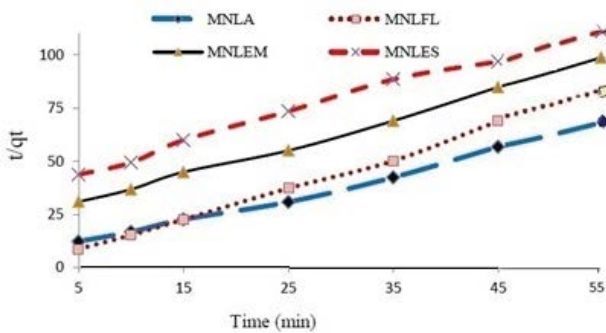
Fig. 10. Fitting of kinetic data of the TC removal to the pseudo-second order kinetic models for MNLES, MNLEM (adsorbent mass: 0.02 g (1 g L^{-1})) and MNLA, MNLFL (adsorbent mass: 0.01 g (0.5 g L^{-1})) (pH = 7; C_{TC} = 44 mg L^{-1}).
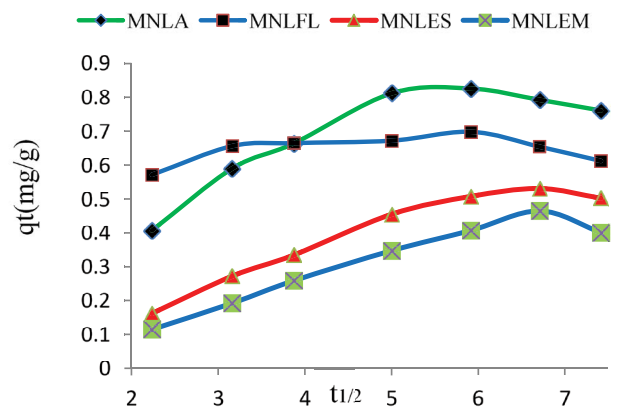
Fig. 11. Intraparticle diffusion model of TC removal for all adsorbents (C_{TC} = 44 mg L^{-1}; V = 20 mL).

Table 1
The values of parameters obtained by different kinetic models

Kinetic models	Parameters	MNLES	MNLEM	MNLFL	MNLA
			TC		
Pseudo-first-order	K_1 (min^{-1})	0.056	0.049	0.5089	0.13
	$q_{e,cal}$ (mg g^{-1})	0.107	0.1419	0.168	0.009
	R^2	0.6328	0.624	0.5	0.4985
Pseudo-second-order	K_2 (g mg^{-1} min^{-1})	0.046	0.073	4.08	0.203
	$q_{e,cal}$ (mg g^{-1})	0.749	0.755	0.676	0.920
	R^2	0.9977	0.9958	0.9968	0.9912
Elovich	β	6.238	5.69	24.75	5.243
	α	0.058	0.085	2.3×10^4	0.373
	R^2	0.9885	0.9931	0.6036	0.9217

Table 2
The results of adsorption isotherms

Isotherm models	Parameters	MNLFL	MNLA	MNLES	MNLEM
	q_{max} (mg g^{-1})	29.94	22.98	25.64	39.84
Langmuir	R^2	0.9932	0.9991	0.7994	0.9956
	K_L (L mg^{-1})	−10.12	1.26	0.115	−0.025
	K_F (mg g^{-1})(L g^{-1})$^{1/n}$	11.92	18.07	3.03	1.8×10^3
Freundlich	n	3.62	19.01	1.373	0.551
	R^2	0.777	0.6595	0.9715	0.8905
	R^2	0.7376	0.6424	0.9423	0.6554
Temkin	K_2 (L g^{-1})	11.239	7.6×10^6	0.525	5×10^{-4}
	K_1 (kJ mol^{-1})	5.2541	1.1277	0.172	−0.0018
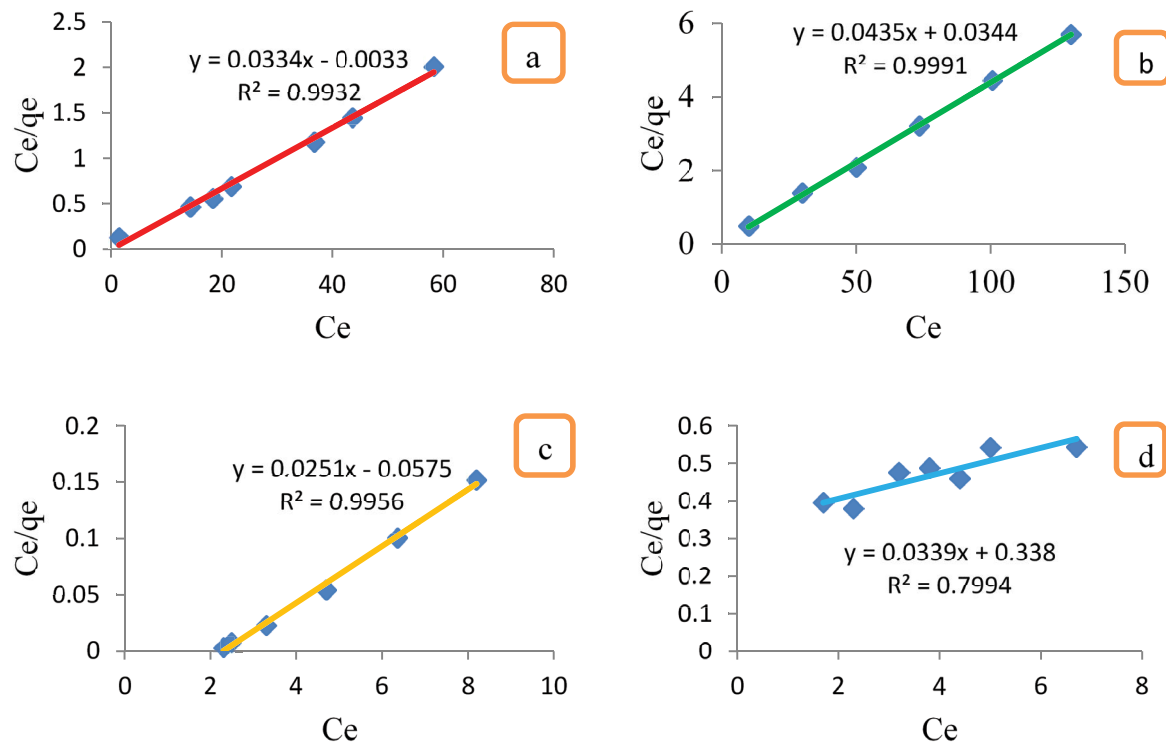
Fig. 12. Langmuir model, a plot of C_e/q_e vs. C_e for (a) MNLFL, (b) MNLA, (c) MNLEM, and (d) MNLES.

TC adsorption occurs on a homogenous surface by monolayer adsorption without any interaction between adsorbed compounds and it shows that all adsorption sites have the same bond to the adsorbed molecules and no transfer of adsorbed occurs at the adsorbent surface. The q_{max} value from the Langmuir model for adsorption of TC were 29.94, 22.98, 25.64 and 39.84 mg g^{-1} for MNLFL, MNLA, MNLES and MNLEM, respectively. All isotherm data are shown in Table 2.

The correlation coefficient for MNLES ($R^2_{Langmuir}$ = 0.7994, $R^2_{Freundlich}$ = 0.9715) showed that adsorption of TC onto the adsorbents follows the Freundlich isotherm more than Langmuir model. The value of q_{max} for adsorption of TC on the MNLES was 25.64 mg g^{-1}. If the value of n^{-1} in Freundlich equation is between 0 to1, it indicates the heterogeneity of surface and desired adsorption level. This parameter

is 0.728 (n = 1.373), therefore TC has proper adsorption on MNLES adsorbent.

In Table 3, different adsorbents that were used in literatures for TC removal were compared in based on their q_{max} values. As can be seen, the proposed magnetite modified natural adsorbents have better q_{max} values for TC removal in comparison to others. This can be related to the structure and functional groups of their surface, as well as their surface modification with magnetic nanoparticles, which creates a large surface with high efficiency and high adsorption speed.

4. Conclusion

The sorption of drugs from aqueous solutions plays a significant role in water pollution control. The MNLES,

Table 3
Comparison of optimum conditions achieved by the proposed sorbent and the other reported sorbents for TC removal in seawage

Adsorbents	Capacity (mg g^{-1})	References
Graphene	39.1	[31]
Zirconium metal–organic framework (UIO-66)	23.1	[32]
Nanocellulose	7.73	[33]
Pumice stone	20.02	[34]
Chitosan	23.92	[35]
Activated carbon	1.98	[36]
Bamboo charcoal	23.5	[37]
Fe_3O_4	10.989	[38]
MNLF	29.94	This work
MNLA	22.98	This work
MNLES	25.64	This work
MNLEM	39.84	This work

MNLEM, MNLA and MNLFL are synthesized easily. Due to their high surface areas, high adsorption capacity can be achieved using magnetic nanoparticles loaded them. For this purpose, the utilization of the MNLES, MNLEM, MNLA and MNLFL as efficient adsorbents was successfully carried out for removal of TC. The adsorption followed the pseudo-second-order kinetic model, suggesting chemisorption mechanism. The fit of the Langmuir isotherm model on the TC adsorption data of MNLEM, MNLA and MNLFL in the present system shows the formation of a monolayer covering of the adsorbate at the outer space of the adsorbent. For MNLES, adsorption data of TC were fitted well to the Freundlich model. The data reported here should be useful for the design and fabrication of an economically treatment process for TC adsorption in industrial effluents.

References

[1] A.U. Rahmah, S. Harimurti, A.A. Omar, T. Murugesan, Optimization of oxytetracycline degradation inside UV/H$_2$O$_2$ reactor using Box-Behnken experimental design, J. Appl. Sci., 12 (2012) 1154–1159.

[2] K.P. Singh, A.K. Singh, U.V. Singh, P. Verma, Optimizing removal of ibuprofen from water by magnetic nanocomposite using Box–Behnken design, Environ. Sci. Pollut. Res., 19 (2012) 724–738.

[3] N. Le-Minh, S.J. Khan, J.E. Drewes, R.M. Stuetz, Fate of antibiotics during municipal water recycling treatment processes, Water Res., 15 (2010) 4295–4323.

[4] S. Rakshit, D. Sarkar, E.J. Elzinga, P. Punamiya, R. Datta, Surface complexation of oxytetracycline by magnetite: effect of solution properties, Vadose Zone J., 13 (2014) 1–10.

[5] S. Rakshit, E.J. Elzinga, R. Datta, D. Sarkar, In situ attenuated total reflectance Fourier-transform infrared study of oxytetracycline sorption on magnetite, J. Environ. Qual., 42 (2013) 822–827.

[6] D. Zhang, H.Y. Niu, X.L. Zhang, Z.F. Meng, Y.Q. Cai, Strong adsorption of chlorotetracycline on magnetite nanoparticles, J. Hazard. Mater., 192 (2011) 1088–1093.

[7] L.L. Ji, F.L. Liu, Z.Y. Xu, S.R. Zheng, D.Q. Zhu, Adsorption of pharmaceutical antibiotics on template-synthesized ordered micro- and mesoporous carbons, Environ. Sci. Technol., 8 (2010) 3116–3122.

[8] Y. Gao, Y. Li, L. Zhang, H. Huang, J.J. Hu, S.M. Shah, X.G. Su, Adsorption and removal of tetracycline antibiotics from aqueous solution by graphene oxide, J. Colloid Interface Sci., 368 (2012) 540–546.

[9] M.C. Zhang, A.M. Li, Q. Zhou, C.D. Shuang, W.W. Zhou, M.Q. Wang, Effect of pore size distribution on tetracycline adsorption using magnetic hypercrosslinked resins, Microporous Mesoporous Mater., 184 (2014) 105–111.

[10] A.L.P.F. Caroni, C.R.M. de Lima, M.R. Pereira, J.L.C. Fonseca, Tetracycline adsorption on chitosan: a mechanistic description based on mass uptake and zeta potential measurements, Colloids Surf., B, 100 (2012) 222–228.

[11] N. Liu, M.-X. Wang, M.-M. Liu, F. Liu, L. Weng, L.K. Koopal, W.-F. Tan, Sorption of tetracycline on organo-montmorillonites, J. Hazard. Mater., 225–226 (2012) 28–35.

[12] R. Sivashankar, A.B. Sathya, K. Vasantharaj, V. Sivasubramanian, Magnetic composite an environmental super adsorbent for dye sequestration – a review, Environ. Nanotechnol. Monit. Manage., 1–2 (2014) 36–49.

[13] F. Shariati, Sh. Shariati, M.A. Amiri Moghaddam, Application of magnetite nanoparticles modified azolla as an adsorbent for removal of reactive yellow dye from aqueous solutions, Desal. Water Treat., 212 (2021) 323–332.

[14] M. Herlekar, S. Barve, R. Kumar, Plant-mediated green synthesis of iron nanoparticles, J. Nanopart., 2014 (2014) 140614, doi: 10.1155/2014/140614.

[15] N. Besharati, N. Alizadeh, Sh. Shariati, Removal of cationic dye methylene blue (MB) from aqueous solution by coffee and peanut husk modified with magnetite iron oxide nanoparticles, J. Mex. Chem. Soc., 62 (2018) 110–124.

[16] Sh. Shariati, M. Faraji, Y. Yamini, A.A. Rajabi, Fe$_3$O$_4$ magnetic nanoparticles modified with sodium dodecyl sulfate for removal of safranin O dye from aqueous solutions, Desalination, 270 (2011) 160–165.

[17] S. Toutounchi, Sh. Shariati, K. Mahanpoor, Sulfonic acid functionalized magnetite nanomesoporous carbons for removal of Safranin O from aqueous solutions, Desal. Water Treat., 153 (2019) 253–363.

[18] J.N. Park, K.J. An, Y.S. Hwang, J.-G. Park, H.-J. Noh, J.-Y. Kim, J.-H. Park, N.-M. Hwang, T.W. Hyeon, Ultra-large-scale syntheses of monodisperse nanocrystals, Nat. Mater., 3 (2004) 891–895.

[19] J.H. Jang, H.B. Lim, Characterization and analytical application of surface modified magnetic nanoparticles, Microchem. J., 94 (2010) 148–158.

[20] A.R. Yari, G. Majidi, M. Tanhaye Reshvanloo, M. Ansari, S. Nazari, M. Emami Kale Sar, M. Khazaei, M.S. Tabatabai-Majd, Using eggshell in Acid Orange 2 dye removal from aqueous solution, Iranian J. Health Sci., 3 (2015) 38–45.

[21] T.V.N. Padmesh, K. Vijayaraghavan, G. Sekaran, M. Velan, Batch and column studies on biosorption of acid dyes on fresh water macro alga azolla *filiculoides*, J. Hazard. Mater., 125 (2005) 121–129.

[22] H. Benaïssa, Removal of cadmium Ions by sorption from aqueous solutions using low-cost materials, Thirteenth International Water Technology Conference, IWTC 13 2009, Hurghada, Egypt, 2009.

[23] R.A. Figueroa, A. Leonard, A.A. Mackay, Modeling tetracycline antibiotic sorption to clays, Environ. Sci. Technol., 38 (2004) 476–483.

[24] Sh. Shariati, Y. Yamini, A. Esrafili, Carrier mediated hollow fiber liquid phase microextraction combined with HPLC-UV for preconcentration and determination of some tetracycline antibiotics, J. Chromatogr. B, 877 (2009) 393–400.

[25] D. Liu, N. Song, W. Feng, Q. Jia, Synthesis of graphene oxide functionalized surface-imprinted polymer for the preconcentration of tetracycline antibiotics, R. Soc. Chem. Adv., 6 (2016) 11742–11748.

[26] P. Raeiatbin, Y.S. Açıkel, Removal of tetracycline by magnetic chitosan nanoparticles from medical wastewaters, Desal. Water Treat., 73 (2017) 380–388.

[27] X.J. Hu, Y.L. Zhao, H. Wang, X.F. Tan, Y.X. Yang, Y.G. Liu, Efficient removal of tetracycline from aqueous media with a

Fe$_3$O$_4$ nanoparticles@graphene oxide nanosheets assembly, Int. J. Environ. Res. Public Health., 14 (2017) 1495, doi: 10.3390/ijerph14121495.

[28] I. Langmuir, The adsorption of gases on plane surfaces of glass, mica and platinum, Am. Chem. Soc., 40 (1918) 1361–1403.

[29] H.M.F. Freundlich, Over the adsorption in solution, Z. Phys. Chem., 57 (1906) 385–470.

[30] M.J. Temkin, V. Pyzhev, Recent modifications to Langmuir isotherms, Acta Physiol. Chem. USSR, 12 (1940) 271.

[31] Y.X. Lin, S. Xu, J. Li, Fast and highly efficient tetracyclines removal from environmental waters by graphene oxide functionalized magnetic particles, Chem. Eng. J., 225 (2013) 679–685.

[32] C.Q. Chen, D.Z. Chen, S.S. Xie, H.Y. Quan, X.B. Luo, L. Guo, Adsorption behaviors of organic micropollutants on zirconium metal–organic framework UiO-66: analysis of surface interactions, ACS Appl. Mater. Interfaces, 9 (2017) 41043–41054.

[33] M. Rathod, S. Haldar, S. Basha, Nanocrystalline cellulose for removal of tetracycline hydrochloride from water via biosorption: equilibrium, kinetic and thermodynamic studies, Ecol. Eng., 84 (2015) 240–249.

[34] U.A. Guler, M. Sarioglu, Removal of tetracycline from wastewater using pumice stone: equilibrium, kinetic and thermodynamic studies, J. Environ. Health Sci. Eng., 12 (2014) 79, doi: 10.1186/2052-336X-12-79.

[35] J. Kang, H.J. Liu, Y.-M. Zheng, J.H. Qu, J.P. Chen, Systematic study of synergistic and antagonistic effects on adsorption of tetracycline and copper onto a chitosan, J. Colloid Interface Sci., 344 (2010) 117–125.

[36] H.R. Pouretedal, N. Sadegh, Effective removal of Amoxicillin, Cephalexin, Tetracycline and Penicillin G from aqueous solutions using activated carbon nanoparticles prepared from vine wood, J. Water Process Eng., 1 (2014) 64–73.

[37] P. Liao, Z.Y. Zhan, J. Dai, X.H. Wu, W.B. Zhang, K. Wang, S.H. Yuan, Adsorption of tetracycline and chloramphenicol in aqueous solutions by bamboo charcoal: a batch and fixed-bed column study, Chem. Eng. J., 228 (2013) 496–505.

[38] M. Stan, I. Lung, M.-L. Soran, C. Leostean, A. Popa, M. Stefan, M.D. Lazar, O. Opris, T.-D. Silipas, A.S. Porav, Removal of antibiotics from aqueous solutions by green synthesized magnetite nanoparticles with selected agro-waste extracts, Process Saf. Environ. Prot., 107 (2017) 357–372.